Review of the Effect of ESD in MEMS

William D. Greason
Department of Electrical and Computer Engineering
Faculty of Engineering
University of Western Ontario
London Ontario Canada N6A 5B9

tel: 519 661-2111 ext. 88334
fax: 519 850-2436
email: wgreason@uwo.ca

***Abstract* - A review is presented of the effect of electrostatic discharge (ESD) on the operation of capacitive microelectromechanical systems (MEMS) structures. Charge injected into the devices can result in failures due to air gap breakdown, stiction, dielectric breakdown and a no operation mode. The dynamic effects of leaky dielectric layers and air gap space charge are also examined.**

I. INTRODUCTION

Microelectromechanical systems (MEMS) which include micro-gap assemblies are inherently very sensitive to electrostatic discharge (ESD). Charge injection into a MEMS structure can result in reliability concerns due to the stiction phenomenon and dielectric breakdown [1-14]. Stiction (a subtraction of "static friction") refers to the phenomenon where microscopic structures tend to adhere to each other when their surfaces come into contact. Electrostatic force due to the charged dielectric layer of a MEMS structure is considered to be the prime cause of stiction. Dielectric layers can become charged due to ESD, triboelectrification and charge injection caused by the high electric fields present during operation. Discharge events in capacitive dielectric layers can also result in leaky dielectric layers and produce air gap space charge; the dynamic response of the structure may be altered.

II. OBJECTIVES

The objective of this paper is to review the effect of ESD on the operation of capacitive MEMS structures. An electric field model is employed to assess the stiction phenomenon, air gap breakdown and dielectric breakdown due to trapped charge in the dielectric. A model is also presented to analyze the effect of a leaky dielectric layer and air gap space charge on the frequency response of a capacitive MEMS structure.

III. CAPACITIVE MEMS CHARACTERISTICS

The operating principle of a MEMS based RF switch is shown in Figure 1; this is an example of capacitive MEMS technology. The RF MEMS switch [15] consists of a free standing plate suspended by beams above a coplanar waveguide; application of a dc voltage is used to cause the bridge to collapse on top of the dielectric. When the bridge is down, the device behaves as an RF shunt switch for GHz range signals. The structure is a basic parallel plate capacitor with the plate collapse being effected by electrostatic force F_1 controlled by the applied voltage. A dielectric layer is necessary to prevent a short circuit during the collapse of the plates. Typical operating voltages are in the range of 15-80 volts [16-18]; designs have been reported with actuation voltages below 5 volts [19-21]. In typical designs [21,22], the plate area is of the order of 100 x 100 μm^2, the plate spacing is of the order of 1-3 μm and the dielectric thickness is 0.2 μm. When charge is injected and trapped in the dielectric layers in MEMS, a bias force F_2 is created which can oppose or assist the force due to the applied operating voltage. Charge injection can be due to the high electric fields associated with the air gap during plate collapse, triboelectrification between the plate and the dielectric layer or ESD. If the bias force due to the injected charge is sufficient, it can cause the plates to remain in the closed position after removal of the control voltage. This is referred to as stiction. The ratio of these two forces can be used as a figure of merit to assess reliability in MEMS where voltage and charge modes are inherently present.

For a parallel plate capacitor with plate area A, plate separation d, applied voltage V, resulting plate charge Q and medium dielectric constant ε, the electrostatic force is given by [23]:

$$F = \frac{Q^2}{2A\varepsilon} = \frac{\varepsilon A V^2}{2d^2} \qquad (1)$$

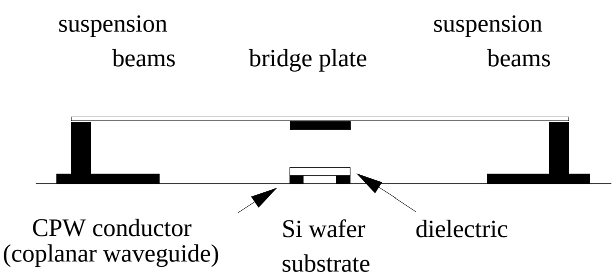

Fig.1 Cross-sectional view of RF MEMS switch

For micro gap assemblies, the modified Paschen's curve presented in Figure 2 has been shown to apply [24]. In this analysis, a linear relation between breakdown voltage and gap will be assumed in the region below approximately 4 μm; as shown in Figure 2, the slope in this region is 7.5 x 10^7 V/m. Beyond 4 μm, the slope becomes 6.2 x 10^4 V/cm; beyond 100 μm, the slope decreases to 3.0 x 10^4 V/cm.

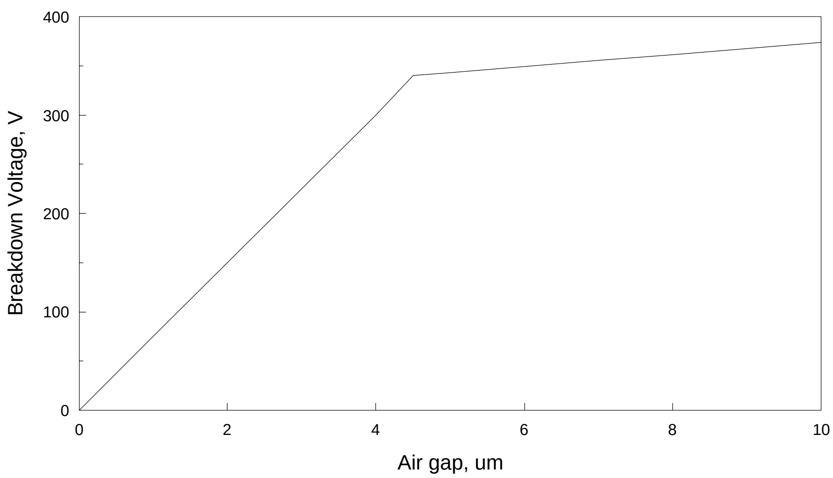

Fig.2 Breakdown voltage in air vs gap

IV. CHARGE INJECTION MODEL

Consider the basic parallel plate model of a capacitive MEMS structure shown in Figure 3. The upper electrode to be displaced by the application of control voltage V_0 has a plate area A and is separated from the fixed reference plate by a distance d. The gap medium is assumed to be air with a permittivity ε_0. Attached to the bottom electrode is a thin dielectric layer of thickness d_0 and dielectric constant k. In this analysis, charge Q_i due to an ESD event is injected into the top electrode, transferred across the air gap due to breakdown and trapped in the dielectric layer on the bottom electrode of the MEMS structure. The total capacitance of the structure is [25]:

$$C_T = \frac{C_1 C_2}{C_1 + C_2} \qquad (2)$$

C_1 is the capacitance of the air gap; C_2 is the capacitance of the dielectric layer.

$$C_1 = \frac{\varepsilon_0 A}{d} \qquad (3)$$

$$C_2 = \frac{k\varepsilon_0 A}{d_0} \qquad (4)$$

The potential developed across the structure due to the injected charge Q_i on the top electrode is:

$$V_0 = \frac{Q_i}{C_T} \qquad (5)$$

This potential is distributed as V_1 and V_2 across the air gap and dielectric layer respectively as:

$$V_1 = V_0 \frac{C_2}{C_1 + C_2} \quad (6)$$

$$V_2 = V_0 \frac{C_1}{C_1 + C_2} \quad (7)$$

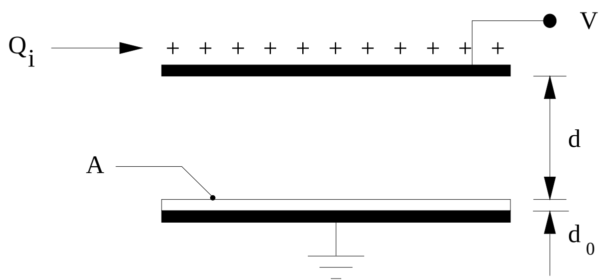

Fig.3 Parallel plate model for capacitive MEMS

Consider a typical MEMS switch with a plate area 100 x 100 μm^2, with an air gap of 3 μm and a dielectric layer of thickness 0.2 μm fabricated from either silicon dioxide (SiO_2) or silicon nitride (Si_3N_4). The following properties apply [26]:

SiO_2: dielectric constant, 3.9; dielectric strength, 10^7V/cm
Si_3N_4: dielectric constant, 7.5; dielectric strength, 10^7V/cm

Since the dielectric thickness d_0 is much smaller than the air gap d, $C_2 >> C_1$ and the following approximations result:

$$C_T \approx C_1 \quad (8)$$

$$V_1 \approx V_0 \quad (9)$$

The resulting potential due to the injected charge is mainly dropped across the air gap. For a gap of 3 μm, the breakdown voltage from the modified Paschen's curve is approximately 300V. Since $C_1 = 3 \times 10^{-14}$F, an injected charge of about 10×10^{-12}C is sufficient for the air gap to breakdown; the injected charge in then transferred to the dielectric layer where it is assumed to be trapped.

In this analysis, for a given gap spacing, it will be assumed that the control voltage is the maximum voltage predicted by the modified Paschen's curve. The slope k_1 of the curve in the region below 4μm is 7.5×10^7 V/m.

V. ELECTRIC FIELD MODEL

The possible failure mode which is analyzed here relates to the breakdown of the dielectric layer in a MEMS structure due to trapped charge. It is assumed the charge Q injected into the MEMS structure by ESD is transferred to the dielectric layer as a result of a breakdown of the air gap; the charge is assumed to be trapped in the dielectric layer. The model shown in Figure 4 is used for the analysis. V_0 is the control voltage applied to the upper plate; the air gap separation is the variable x; the thickness of the dielectric layer with dielectric constant k is a. The surface charge density of the injected charge on the dielectric layer is $\sigma C/m^2$. The electric fields in the air gap and dielectric are E_B and E_A respectively.

The fields in the regions above and below the charge layer satisfy the boundary conditions [27]:

$$E_A a \quad + \quad E_B x \quad = \quad V_0 \tag{10}$$

$$k\varepsilon_0 E_a \quad + \quad \varepsilon_0 E_B \quad = \quad \sigma \tag{11}$$

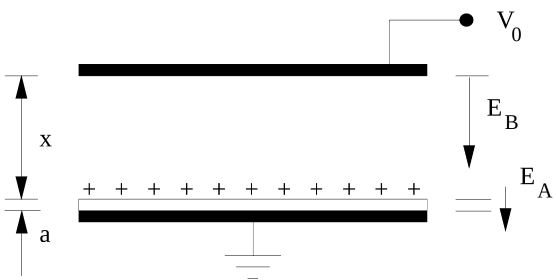

Fig.4 Electric field model for capacitive MEMS structure

The solutions for the electric fields in the air gap (E_B) and the dielectric (E_A) , and the potential drops across the air gap (V_B) and the dielectric layer (V_A) are:

$$E_A \quad = \quad \frac{V_0}{a} \; \frac{1}{1 + kx/a} \quad + \quad \frac{\sigma}{k\varepsilon_0} \; \frac{1}{1 + a/kx} \tag{12}$$

$$V_A \quad = \quad V_0 \; \frac{1}{1 + kx/a} \quad + \quad \frac{\sigma a}{k\varepsilon_0} \; \frac{1}{1 + a/kx} \tag{13}$$

$$E_B \quad = \quad \frac{k\,V_0}{a} \; \frac{1}{1 + kx/a} \quad - \quad \frac{\sigma}{\varepsilon_0} \; \frac{1}{1 + kx/a} \tag{14}$$

$$V_B \quad = \quad V_0 \; \frac{1}{1 + a/kx} \quad - \quad \frac{\sigma a}{k\varepsilon_0} \; \frac{1}{1 + a/kx} \tag{15}$$

These equations permit an analyses of the electric fields and voltage drops in the air gap and dielectric layer associated with a MEMS parallel plate structure. The modes of analysis include: Normal operating mode ($V = V_0$, $\sigma = 0$); Charged dielectric only ($V = 0$, $\sigma = \sigma_0$); Normal operating mode with charged dielectric ($V = V_0$, $\sigma = \sigma_0$). The limiting cases include: plates open: $x \gg a$; plates closed: $x \ll a$.

From a review of equations (12) to (15), a/kx is chosen as the variable which defines the state of the plates. For $a/kx \ll 1$, the plates are open; for $a/kx \gg 1$, the plates are closed. Graphs for the contribution to the voltage drop across the air gap due to the control voltage and the trapped charge in the dielectric are presented in Figures 5 and 6 respectively; graphs for the contribution to the electric field in the dielectric layer due to the control voltage and the trapped charge in the dielectric are presented in Figures 7 and 8 respectively.

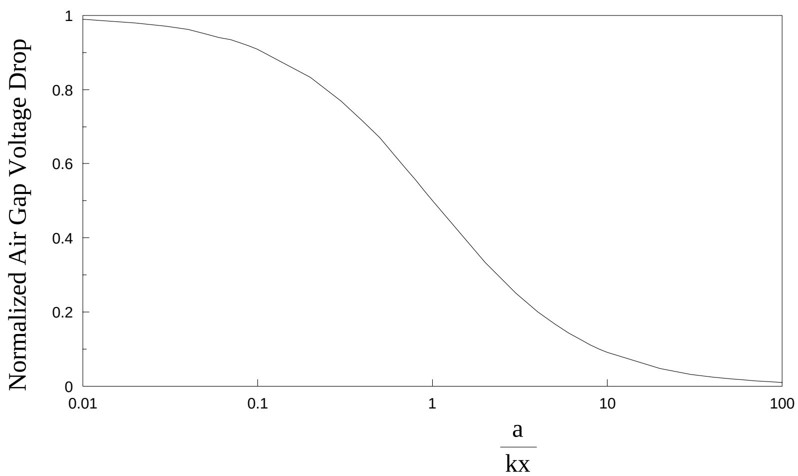

Fig.5 Air gap voltage drop due to control voltage normalized to V_0 vs gap factor a/kx

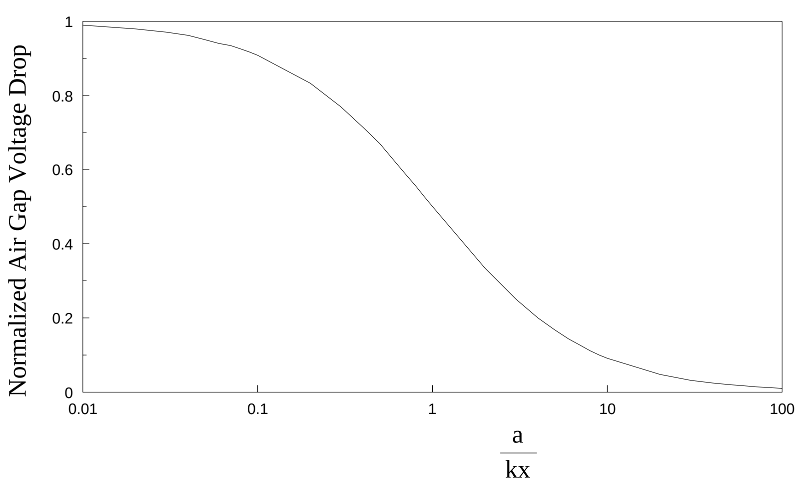

Fig.6 Air gap voltage drop due to surface charge density normalized to $(\sigma a)/(k\varepsilon_0)$ vs gap factor a/kx

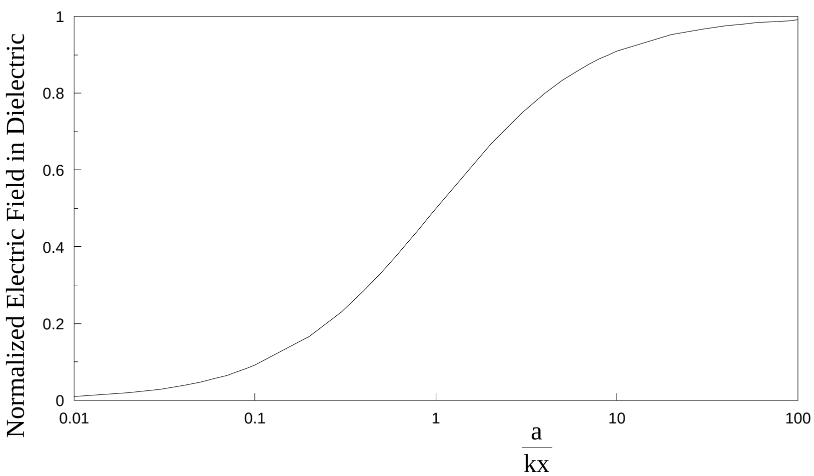

Fig.7 Electric field in dielectric due to control voltage normalized to V_0/a vs gap factor a/kx

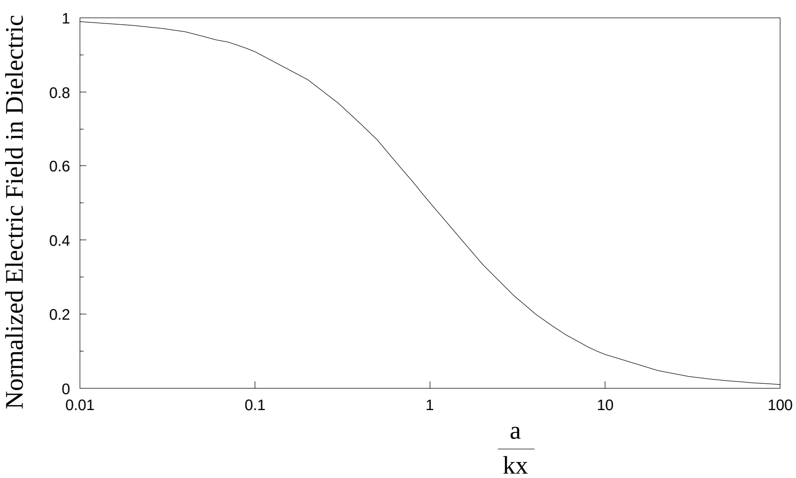

Fig.8 Electric field in dielectric due to surface charge density normalized to $\sigma/(k\varepsilon_0)$ vs gap factor a/kx

Calculations will be done for a typical test structure; the following values of the various parameters will be used.

Maximum air gap spacing: 3 μm
Dielectric thickness: 0.2 μm
Dielectric constant: 5
Breakdown strength of dielectric: 1×10^9 V/m
Breakdown strength of air (slope of modified Paschen's curve): 7.5×10^7 V/m
Plate area: 100x100 μm^2.

A. Dielectric Surface Charge Only: Voltage Drops

The general expression for the air gap voltage drop is:

$$V_B \quad = \quad V_0 \quad \frac{1}{1+a/kx} \quad - \quad \frac{\sigma a}{k\varepsilon_0} \quad \frac{1}{1+a/kx} \qquad (16)$$

Both terms in this expression have a maximum when the switch is open and decrease as the switch is closed. Equating the two terms will yield the surface charge density which gives the same voltage drop as due to the control voltage V_0. This can be interpreted as the condition for the onset of stiction.

$$V_0 \quad \frac{1}{1+a/kx} \quad = \quad \frac{\sigma a}{k\varepsilon_0} \quad \frac{1}{1+a/kx} \qquad (17)$$

$$\sigma \quad = \quad \frac{V_0 k \varepsilon_0}{a} \qquad (18)$$

For the test structure, this gives $\sigma = 2.2\text{x}10^{-3}$ C/m^2.

Stiction is defined as the failure for the plates to release upon removal of the control voltage V_0. It is caused by the air gap voltage drop due to σ being of the same magnitude as the voltage drop due to V_0.

With the plates open, another interpretation of equation (16) can be made. For σ positive and V_0 positive, it is noted that the polarity of the voltage drop due to σ is opposite in polarity to the voltage drop due to V_0. It is then possible that the net air gap voltage approaches zero which would imply a no operation mode for the switch with the application of the control voltage. This will be defined as the no op mode.

B. Dielectric Surface Charge Only: Electric Fields

In this case, the control voltage $V_0 = 0$ and the dielectric surface charge density is σ.

For the air gap:

$$E_B \quad = \quad -\frac{\sigma}{\varepsilon_0} \quad \frac{1}{1+kx/a} \qquad (19)$$

For the dielectric layer:

$$E_A \quad = \quad \frac{\sigma}{k\varepsilon_0} \quad \frac{1}{1+a/kx} \qquad (20)$$

The maximum electric field E_A in the dielectric due to σ is realized when the switch is open.

$$E_A \quad = \quad \frac{\sigma}{k\varepsilon_0} \qquad (21)$$

It is possible to solve for the surface charge density for dielectric breakdown.

$$\sigma \quad = \quad k\varepsilon_0 E_{BD}$$

For the test example, $\sigma = 44.25 \text{ x } 10^{-3}$ C/m^2

For the switch open, the electric field E_B in the air gap is:

$$E_B = \frac{\sigma}{k\varepsilon_0} \frac{a}{x} \tag{22}$$

For the example, $E_B = 6.67 \times 10^7$ V/m. This is less than the breakdown value of 7.5×10^7 V/m for the modified Paschen's curve. This example shows that the dielectric can breakdown while the air gap does not.

The electric field E_A in the dielectric can also be written as:

$$E_A = \frac{Q}{k\varepsilon_0 A} \tag{23}$$

Two additional observations are made. The electric field increases in proportion to the total charge Q injected, which could be the result of single or multiple discharge events. As the structures are scaled, the electric field will increase in proportion to 1/A and the critical charge for breakdown will decrease in proportion to the plate area A.

An estimate of the critical charge Q_{BD} for breakdown can be made. The following values are assumed: k = 5, A = 100x100 μm^2, $E_{BD} = 10^7$ V/cm. Then $Q_{BD} = k\varepsilon_0 A E_{BD} = 4.4 \times 10^{-10}$C.

VI. IMPEDANCE ANALYSIS MODEL

A. MEMS equivalent circuit

The equivalent circuit used in the analysis is shown in Figure 9. R_1 and C_1 are the resistance and capacitance respectively of the air gap. Under normal conditions, R_1 is due to the natural conductivity of air; the value is reduced due to space charge which can result from breakdown events across the air gap due to ESD. R_2 and C_2 are the resistance and capacitance respectively of the dielectric layer. Under normal conditions, R_2 is due to the normal resistivity of the dielectric; the value is reduced either deliberately during manufacture to assist in the dissipation of surface charge or during operation as the result of repeated breakdown events in the dielectric.

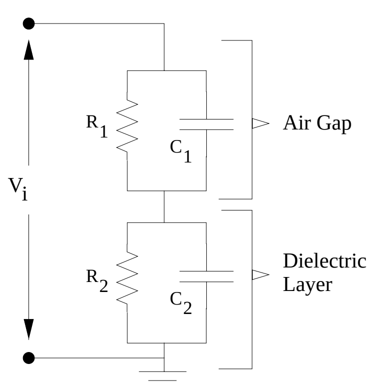

Fig.9 Equivalent circuit of capacitive MEMS structure

B. Test Structure

A typical MEMS switch [21,28] has a plate area of 100 x 100 μm^2 with an air gap of 3 μm and a dielectric layer of thickness 0.2 μm. Usually either silicon dioxide (SiO_2) or silicon nitride (Si_3N_4) are used in the fabrication of the layer. An average of their material properties [26] will be used in computations for the test cell as follows: dielectric constant - 5; dielectric strength - 10^7 V/cm; volume resistivity - 10^{14} Ω.cm. For the air gap, a typical conductivity value of 2 x 10^{-14} $\Omega^{-1}.m^{-1}$ will be used [29].

In this analysis, the switch will be assumed to be in the open state. The calculated values of the elements in the equivalent circuit of the test cell are:

$$R_1 = 1.5 \times 10^{16}\ \Omega;\ C_1 = 2.95 \times 10^{-14}\ F$$
$$R_2 = 2 \times 10^{13}\ \Omega;\ C_2 = 2.2 \times 10^{-12}\ F$$

C. Frequency Domain Analysis

The equivalent circuit shown in Figure 10 will be used to determine the transfer function of the MEMS structure. The transfer function is defined as the ratio of the air gap voltage drop V_0 to the control voltage V_i. By voltage division,

$$\frac{V_o}{V_i} = \frac{Z_1}{Z_1 + Z_2} \tag{24}$$

Z_1 is the complex impedance of R_1 in parallel with C_1; Z_2 is the complex impedance of R_2 in parallel with C_2.

The straight line approximation technique is used to estimate impedances Z_1 and Z_2 as a function of frequency. An examination of the graphical presentation of Z_1 and Z_2 is then used to determine the transfer function of the MEMS cell as a function of frequency.

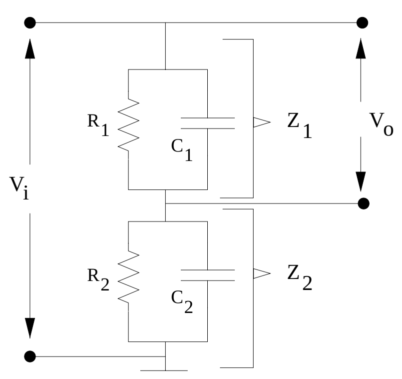

Fig.10 Impedance analysis model

1) Case I: Leaky Dielectric

The effective resistance R_2 of the dielectric layer can be decreased either through selection of material properties at manufacture or by dielectric breakdown initiated by surface charge transferred across the air gap in ESD events. The straight line approximations for Z_1 and Z_2 are shown in Figure 11. At any frequency, equation (24) applies.

For $f < f_1$, $\dfrac{V_o}{V_i} = 1$ since $R_1 \gg R_2$

For $f_1 < f < f_2$ $\dfrac{V_o}{V_i} = 1$ since $1/\omega C_1 \gg R_2$

For $f > f_2$, $\dfrac{V_o}{V_i} = 1$ since $1/\omega C_1 \gg 1/\omega C_2$

For the test cell, the calculated corner frequencies are $f_1 = 3.6\text{x}10^{-4}$ Hz and $f_2 = 3.6\text{x}10^{-3}$ Hz. For a MEMS structure, the frequency region of interest relates to the time domain characteristics of the control voltage V_i. The effective bandwidth of a rectangular pulse of length T is [30]:

$$B_{eff} = \frac{1}{T} \tag{25}$$

An analysis of the frequency domain response of the air gap voltage can be effected through an examination of the straight line approximations for Z_1 and Z_2. As R_2 is decreased, the corner frequency f_2 for Z_2 increases. For each decrease by an order of 10 for R_2, f_2 increases by one decade. However, for the example shown, the air gap voltage drop V_o is equal to the control voltage V_i independent of frequency.

It has been shown previously that the accumulation of surface charge on the dielectric can cause stiction and dielectric breakdown. The relaxation time for the dielectric is given by:

$$\tau = R_2 C_2 \tag{26}$$

By proper design, the relaxation time can be chosen to prevent the accumulation of surface charge which would interfere with the operation time of the structure. For example, for a relaxation time of 1s, $R_2 = 4.6\text{x}10^{11}\ \Omega$; the corner frequency f_2 becomes $1.6\text{x}10^{-1}$ Hz.

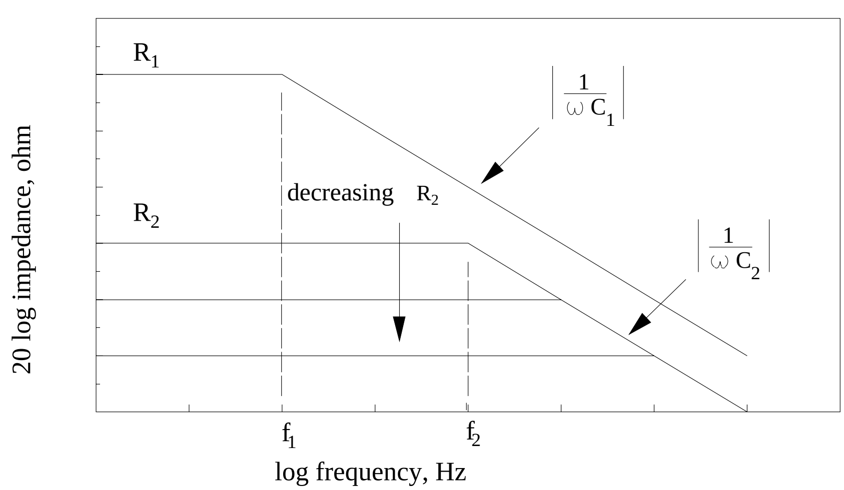

Fig.11 Cell impedances vs frequency for leaky dielectric

2) Case IIa: Low Density Space Charge

The effective resistance R_1 of the air gap can be decreased by space charge which results from a breakdown across the air gap due to an ESD event. The straight line approximations for Z_1 and Z_2 are shown in Figure 12. As R_1 decreases, the corner frequency f_1 for Z_1 increases. For each decrease by an order of 10 for R_1, f_1 increases by one decade. For low density space charge, the analysis presented for Case I applies; the air gap voltage drop V_o is equal to the control voltage V_i independent of frequency.

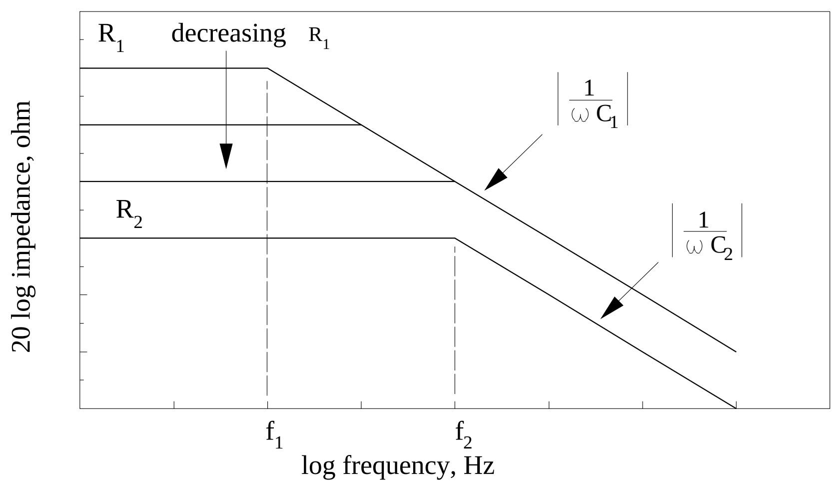

Fig.12 Cell impedances vs frequency for low density space charge in air gap

3) Case IIb: High Density Space Charge

The straight line approximations for Z_1 and Z_2 for the case of high space charge density are shown in Figure 13. Calculations can show that only a very small fraction of the charge transferred in an ESD event can yield a space charge sufficient to dramatically reduce the columnar resistance of the air gap. The columnar resistance [29] is the effective resistance of a micro column of space charge introduced by air gap breakdown events.

$$\text{For} \quad f < f_1, \quad \frac{V_o}{V_i} = \frac{R_1}{R_2} < 1$$

This is considered to be the condition for no operation since the air gap voltage is reduced and is not sufficient to effect closure of the switch.

$$\text{For} \quad f_1 < f < f_2, \quad \frac{V_o}{V_i} = \frac{R_1}{1/\omega C_2}$$

This is considered to be an indeterminate state since the air gap voltage may be reduced sufficiently to cause no closure of the switch.

$$\text{For} \quad f > f_2, \quad \frac{V_o}{V_i} = \frac{C_2}{C_1} = 1 \quad \text{since} \quad C_2 > C_1$$

The air gap voltage is equal to the control voltage; normal operation and closure of the switch will result. In the above analysis, a corner frequency $f_2 = 1$ Hz corresponds a control voltage pulse width of 1s. The columnar resistance for this corner frequency is $R_C = R_2 = 1x10^{10}\ \Omega$.

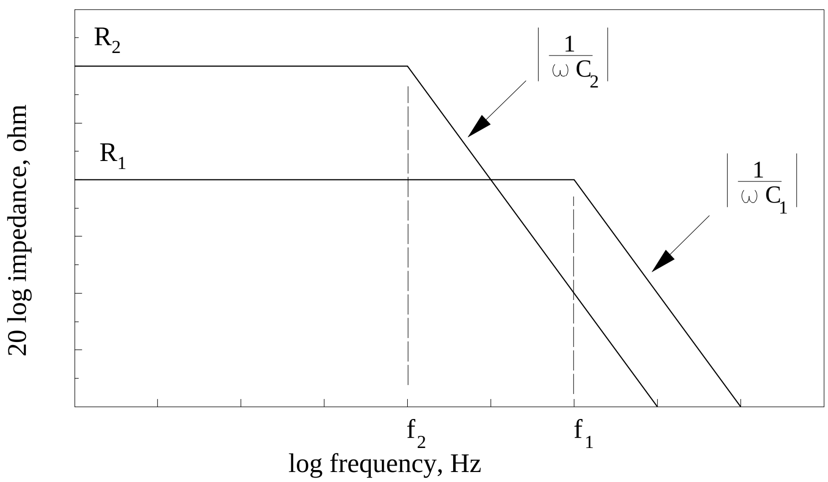

Fig.13 Cell impedances vs frequency for high density space charge in air gap

VII. SUMMARY

A review has been presented for the effect of ESD on the operation of MEMS. Charge injection processes due to air gap discharges, triboelectrification and high electric fields associated with operating voltages have been analyzed; reliability concerns associated with stiction, dielectric breakdown and on operation states have been evaluated. A methodology to study the effect of leaky dielectric layers and air gap space charge on the dynamic response of a capacitive MEMS structure has been introduced.

REFERENCES

[1] R. Ranganathan, G. Sivakumar, R. Gale and T. Dallas, "Characterization of stiction accrual in a MEMS", Journal of Microelectromechanical Systems, Vol. 18, No. 5, October 2009, pp. 1149-1159.

[2] P. Czarnecki, X. Rottenberg, P. Soussan, P. Ekkels, P. Muller, P. Nolmans, W. De Raedt, H.A.C. Tilmans, R. Puers, L. Marchand and I. De Wolf, "Effect of substrate charging on the reliability of capacitive RF MEMS switches", Sensors and Actuators A, Vol. 154, No. 2, September 2009, pp. 261-268.

[3] J. Ruan, N. Nolhier, G.J. Papaioannou, D. Tremouilles, V. Puyal, C. Villeneuve, T. Idda, F. Coccetti and R. Plana, "Accelerated lifetime test of RF-MEMS switches under ESD stress", Microelectronics Reliability, Vol. 49, No. 9-11, September 2009, pp. 1256-1259.

[4] D.M. Tanner, "MEMS reliability: Where are we now?", Microelectronics Reliability, Vol. 49, No. 9-11, September 2009, pp. 937-940.

[5] U. Zaghloul, G. Papaioannou, F. Coccetti, P. Pons and R. Plana, "Dielectric charging in silicon nitride films for MEMS capacitive switches: Effect of film thickness and deposition conditions", Microelectronics Reliability, Vol. 49, No. 9-11, September 2009, pp. 1309-1314.

[6] J. Ruan, G.J. Papaioannou, N. Nolhier, N. Mauran, M. Bafleur, F. Coccetti and R. Plana, "ESD failure signature in capacitive RF MEMS switches", Microelectronics Reliability, Vol. 48, No. 8-9, August 2008, pp. 1237-1240.

[7] J. Ruan, N. Nolhier, M. Bafleur, L. Bary, F. Coccetti, T. Lisec and R. Plana, "Electrostatic discharge failure analysis of capacitive RF MEMS switches", Microelectronics Reliability, Vol. 47, No. 9-11, September 2007, pp. 1818-1822.

[8] M. Lamhamdi, J. Guastavino, L. Boudou, Y. Segui, P. Pons, L. Bouscayrol and R. Plana, "Charging-effects in RF capacitive switches: Influence of insulating layer composition", Microelectronics Reliability, Vol. 46, No. 9-11, September 2006, pp. 1700-1704.

[9] H. Wolf, H. Gieser, D. Bonfert and M. Hauser, "ESD susceptibility of submicron air gaps", Microelectronics Reliability, Vol. 46, No. 9-11, September 2006, pp. 1587-1590.

[10] M. Exarchos, V. Theonas, P. Pons, G.J. Papaioannou, S. Melle, D. Dubac, F. Coccetti and R. Plana, "Investigation of charging mechanisms in metal-insulator-metal structures", Microelectronics Reliability, Vol. 45, No. 9-11, September 2005, pp. 1782-1785.

[11] S. Melle, D. De Conto, L. Mazenq, D. Dubuc, B. Poussard, C. Bordas, K. Grenier, L. Bary, O. Vendier, J.L. Muraro, J.L. Cazaux and R. Plana, "Failure predictive model of capacitive RF-MEMS", Microelectronics Reliability, Vol. 45, No. 9-11, September 2005, pp. 1770-1775.

[12] J.A. Walraven, "Failure analysis issues in microelectromechanical systems (MEMS)", Microelectronics Reliability, Vol. 45, No. 9-11, September 2005, pp. 1750-1757.

[13] W.M. van Spengen, "MEMS reliability from a failure mechanisms perspective", Microelectronics Reliability, Vol. 43, No. 7, July 2003, pp. 1049-1060.

[14] I. De Wolf and W.M. van Spengen, "Techniques to study the reliability of metal RF MEMS capacitive switches", Microelectronics Reliability, Vol. 42, No. 9-11, September 2002, pp. 1789-1794.

[15] W.M. van Spengen, R. Puers, R. Mertens and I. De Wolf, "A comprehensive model to predict the charging and reliability of capacitive RF MEMS switches", Journal of Micromechanics and Microengineering, Vol. 14, No. 4, April 2004, pp. 514-521.

[16] J.B. Muldavin and G.M. Rebeiz, "High isolation CPW MEMS shunt switches - part 1: modeling", IEEE Transactions on Microwave Theory and Techniques, Vol. 48, No. 6, June 2000, pp. 1045-1052.

[17] J.B. Muldavin and G.M. Rebeiz, "High isolation CPW MEMS shunt switches - part 2: design", IEEE Transactions on Microwave Theory and Techniques, Vol. 48, No. 6, June 2000, pp. 1053-1056.

[18] L.P.B. Katehi, J.F. Harvey and E. Brown, "MEMS and Si micromachined circuits for high-frequency applications", IEEE Transactions on Microwave Theory and Techniques, Vol. 50, No. 3, March 2002, pp. 858-866.

[19] D. Hah, E. Yoon and S. Hong, "A low-voltage actuated micromachined microwave switch using torsion springs and leverage", IEEE Transactions on Microwave Theory and Techniques, Vol. 48, No. 12, December 2000, pp. 2540-2545.

[20] I.-J. Cho, T. Song, S.-H. Baek and E. Yoon, "A low-voltage and low-power RF MEMS series ans shunt switch actuated by a combination of electromagnetic and electrostatic forces", IEEE Transactions on Microwave Theory and Techniques, Vol. 53, No. 7, July 2005, pp. 2450-2457.

[21] S.-D. Lee, B.-C. Jun, S.-D. Kim, H.-C. Park, K.-K. Rhee and K. Mizuno, "An RF-MEMS switch with low-actuation voltage and high reliability", Journal of Micromechanical Systems, Vol. 15, No. 6, December 2006, pp. 1605-1611.

[22] K.D. Leedy, R.E. Strawser, R. Cortez and J.L. Ebel, "Thin-film encapsulated RF MEMS switches", Journal of Microelectromechanical Systems, Vol. 16, No. 2, April 2007, pp 304-309.

[23] C. Cabuz, E.I. Cabuz, T.R. Ohnstein, J. Neus and R. Maboudian, "Factors enhancing the reliability of touch-mode electrostatic actuators", Sensors and Actuators, Vol. 79, 2000, pp. 245-250.

[24] R.M. Schaffert, *Electrophotography*. Focal Press Limited, New York, 1965.

[25] W.H. Hayt, *Engineering Electromagnetics, 4th edition.* McGraw-Hill, NY, 1981.

[26] S.M. Sze, *Physics of Semiconductor Devices, 2nd edition.* John Wiley and Sons, NY, 1981.

[27] J.M. Crowley, *Fundamentals of Applied Electrostatics.* Laplacian Press, Morgan Hill, CA, 1999.

[28] S. Melle, D. De Conto, D. Dubic, K. Grenier, O. Vendier, J.-L. Muraro, J.-L. Cazaux and R. Plana, "Reliability modeling of capacitive RF MEMS", IEEE Transactions on Microwave Theory and Techniques, Vol. 53, No. 11, pp. 3482-3488, November 2005.

[29] J.A. Chalmers, *Atmospheric Electricity*. Pergamon Press, New York, 1957.

[30] R.B. Randall, *Frequency Analysis*, 3rd edition. Bruel & Kjaer, Denmark, 1987.